

Quantum nature of molecular vibrational quenching: Water - molecular hydrogen collisionsLaurent Wiesenfeld¹*Laboratoire Aimé-Cotton, CNRS & Université Paris-Saclay, Orsay, France^{a)}*

(Dated: 13 January 2022)

Rates of conversions of molecular internal energy to and from kinetic energy by means of molecular collision allows to compute collisional line shapes and transport properties of gases. Knowledge of ro-vibrational quenching rates is necessary to connect spectral observations to physical properties of warm astrophysical gasses, including exo-atmospheres. For a system of paramount importance in this context, the vibrational bending mode quenching of H₂O by H₂, we show here that exchange of vibrational to rotational and kinetic energy remains a quantum process, despite the large numbers of quantum levels involved and the large vibrational energy transfer. The excitation of the quantized rotor of the projectile is by far the most effective ro-vibrational quenching path of water. To do so, we use a fully quantum first principle computation, potential and dynamics, converging it at all stages, in a full coupled channel formalisms. We present here rates for the quenching of the first bending mode of ortho-H₂O by ortho H₂, up to 500 K, in a fully converged coupled channels formalism.

^{a)}Electronic mail: laurent.wiesenfeld@universite-paris-saclay.fr

Collisional exchange of energy (internal and kinetic) is a fundamental process leading to the equilibrium between internal temperatures of molecules and kinetic temperature of the gas in which they are immersed¹. There exists many attempts to compute those rates for transport properties, all the way from classical computation (recent examples are^{2,3}) to full quantum ab initio computations⁴. While a large body of investigation deals with collisional rates for astrophysics and planetary science, as described in the next paragraph, the role of internal to kinetic energy exchanges is also crucial in cold molecules physics ($T \sim \text{K to mK}$). In an cold molecular gas, energy exchanges between the molecules observed and with the buffer gas, possibly causing heating of the cold molecules.^{5,6}

The recent surge in interest towards elastic and inelastic collisions stems mainly from precise atmospheric/astrochemical needs.⁷⁻⁹ Most data pertaining to the physical and chemical-physical states of gaseous matter in the Universe come from atomic or molecular spectroscopy. For decades, most of the quantitative information was gained from the rotational lines of ground state molecules, thanks to the high precision, high specificity of rotational spectra in the cm to sub-mm spectral regions^{10,11}.

Because of newer instruments on the ground and thanks to plane- or space-born telescopes, the opacity of the atmosphere to FIR-IR light is progressively overcome, and opens up new opportunities: Microwave (THz frequencies) to Infra Red spectra carry information otherwise unattainable, on the warm interstellar matter and on planetary/cometary atmospheres in the Solar System or in exoplanets. Many molecules are thus nowadays observed in their vibrationally excited states, whether by rotational spectroscopy within those states, or else by observing the FIR-IR lines connecting different ro-vibrational levels¹². Among the molecules observed, water is prominent¹³, being the third most abundant (after H_2 and CO) and the first polyatomic one. The relevance of the ro-vibrational quenching of water is further enhanced by the relatively recent discovery of masing transition of ortho-water, in the transition $\nu_b = 1; 1_{10} \rightarrow 1_{01}$, at $\nu = 658.00 \text{ GHz}$ ¹⁴⁻¹⁶ [Rotational levels of water are labelled $j_{k_a k_c}$; ortho $^1\text{H}_2\text{O}$ (nuclear spin triplet) has $k_a + k_c$ odd; ν_b is the water bending mode quantum number] .

The present approach constitutes, for the author's best knowledge, a first *ab initio* study of quantum ro-vibrational quenching for a polyatomic molecule, that includes rotational states of the projectile. Integrating these new rotational channels increases the magnitude of the vibrational quenching rates (and cross sections) by several orders of magnitude, when compared with earlier work, either classical¹⁷ or quantum^{18,19} . It has always been expected that quantum effects would

dominate the landscape for low collisional energies, comparable to the minimum of the van der Waals potential $|V_{\min}|$ (here, $V_{\min} \sim -250 \text{ cm}^{-1}$)^{20–22}, but quantum aspects are supposed to disappear progressively as the collision energy increases. In a very different context, combustion modelling³, the same assumption is made that there exists a critical temperature $T^* = kT/|V_{\min}|$, above which classical picture is sufficient to describe collisional transport.

We show here that the very different energy scales of water rotations, molecular hydrogen rotation, and water vibration lead to the resurgence of a strong dependence of the cross sections to the quantum levels of H_2 and H_2O involved. This resurgence does not happen for purely rotational energy redistribution: even classical and/or statistical approaches²³ are relevant when a large number of coupled levels interact. It is most significant here, and, to a lesser extent, to collisions involving water and a heavier partner, like N_2 , which is described by a toy model in this work.

While classical and semi-classical methods are certainly of relevance in rotational quenching, it must be recalled that the semi-classical quantization of an asymmetric rotor is problematic²⁴, at least for j small enough so that the two associated levels j_{k_a, k_c} and j_{k_a-1, k_c+1} are clearly distinct.

Computing collisional coefficients for purely rotational transitions has been a nearly continuous endeavour since the pioneering work of Delgarno^{25–32}. The scenario is always the same, and it is the one we pursue here: (i) Computing *ab initio* the interaction potential $V_n(\mathbf{R})$ of the polar molecule and the projectile (\mathbf{R} denotes collectively all necessary coordinates, n are the points where computing is performed), (ii) fitting the n computed points onto a functional form acceptable for dynamics, (iii) running quantum dynamics of the collision pair, and (iv) computing cross-section as a function of collisional energy $\sigma(E)$ or rates as a function of the kinetic temperature of the collider gas $k(T)$.

Thanks to the experience gained in recent precise rotational inelastic scattering computations and of very convincing comparisons of theory with several types of experiments^{20,22,33}, it is safe to deal with ro-vibrational collisional excitation with the same types of methods and basis sets that were used previously, and conduct a fully quantum dynamical approach.

We employ the full dimensional (9 degrees of freedom) water-molecular hydrogen potential energy surface³⁴ (hereafter denoted val08), $V(R, \Omega, \delta r_q)$. This surface includes the 5 intermolecular degrees of freedom (intermolecular distance R and 4 angles Ω to orient one molecule with respect to the other), as well as 4 normal coordinates describing motion around equilibrium position of the molecules, δr_q , $q = 1, \dots, 4$. Details of this surface are in the original paper. Since quantum

dynamics is performed with a quantum time-independent computation of the S-matrix, we need to fit the ab initio points on the relevant S. Green type of mixed coordinates²⁸. Molscat code was used³¹, duly modified to include vibrational modes in the potential expression. We did not include the modification of the kinetic energy due to rovibrational motion³⁵, but restricted ourselves to potential effects, and expressed the potential in coordinates satisfying Eckart conditions. Since we deal only with the first bending mode $v_b = 1$ and low lying rotational levels in the excited vibrational mode, we made the assumption: $|v_b; j_{k_a, k_c}\rangle = |v_b\rangle \otimes |j_{k_a, k_c}\rangle_{v_b}$. The rotational functions are parameterized by the rotational parameters of either $v_b = 0$ ³⁶ or $v_b = 1$, but they are not rovibrational functions. We also averaged the dependance of the potential on the vibrational ground state of H₂.

Time-independent quantum dynamics is performed here on two coupled sets of potential energy surfaces with full dimensional (5D) potentials, including H₂ rotation (denoted by the quantum number j_2), in a converged coupled channels approach. The potentials were obtained by computing the averages of the 9-D potential : $C_{v'_b, v_b}(R, \omega) = \langle v'_b | V(R, \Omega, \delta r_q) | v_b \rangle$ functions, with $v_b, v'_b = 0, 1$ [see val08]. The coupling $W(R)$ matrix is thus written blockwise as (with R the intermolecular distance)³⁷:

$$\Psi''(R) = \left[\begin{pmatrix} W_{11}(R) & V_{01}(R) \\ V_{01}(R) & W_{00}(R) \end{pmatrix} - \begin{pmatrix} k_2^2 \\ k_1^2 \end{pmatrix} \right] \Psi(r) \quad (1)$$

where the $W_{00}(R)$ and $W_{11}(r)$ matrices are formed by using the potential of each vibrational level (including the diagonal contributions), and the non-diagonal rotational terms, bracketed with the relevant spherical harmonic functions²⁸, [val08]. The $V_{01}(R)$ matrix is also given by duly bracketing the $C_{v'_b, v_b}(R, \omega)$ function with the same spherical harmonic functions.

In order to be able to deal with representative (symmetric) matrices of sizes less than 12,000 × 12,000 (the practical limit of OpenMP computing), we further split the computation by treating each total angular momentum value J (recoupling j, j_2, ℓ , the orbital angular momentum) and, if necessary, each inversion symmetry, separately. We used a relatively coarse grid of total energies (E_{tot} from threshold to about 3,000 cm⁻¹), as we are not interested in the detailed resonance behaviour occurring typically at $1 \text{ cm}^{-1} < E_{\text{collision}} < |V_{\text{min}}|$.

We present results for ortho ¹H₂O - ortho ¹H₂ collisions. The present analysis could serve as a basis for the modelling the masing transition of water at 658 GHz^{14,38}; also, ortho H₂ is more abundant than para H₂ at the higher temperatures that we examine. With a large rotational basis set we computed all inelastic cross sections with initial levels $v_b = 1; j_{k_a k_c} = 1_{01}$ up to 3_{21} . Rotational

basis for water is $j(v = 0) \leq 14$; $j(v = 1) \leq 6$; only rotational levels with $E \leq 3500 \text{ cm}^{-1}$ are included. Convergence was reached at higher energies for total angular momentum $J = 28$ to 32.

Next (Fig. 1), we compute quenching cross sections as a function of scattering energy and quenching rates as a function of temperature (inset of Fig. 1). In both figures, we show the total quenching section (or rate) from a series of excited ro-vibrational levels (as described in the caption of Fig. 1) to all $v_b = 0$ levels and constraining to de-excitation (Excluding the $v_b = 0$ levels that are above the $v'_b = 1$ original levels):

$$\sigma_{v'=0 \leftarrow v=1, j_k a k_c}(E) = \sum_{j', k'_a, k'_c} \sigma_{v'=0; j'_k a' k'_c \leftarrow v=1, j_k a k_c}(E), \quad (2)$$

and rates obtained therefrom by averaging over the collisional energy. Fig. 1 shows results for three rotational bases of the H_2 : (i) para- H_2 , $j_2 = 0$, to be compared with the results of¹⁸ (ii) $j_2 = 1$, the usual basis for many computations for collisions between a molecule and ortho- H_2 , (iii) a larger basis for ortho- H_2 , $j_2 = 1, 3$. Full results with all detailed cross sections and rates will be published

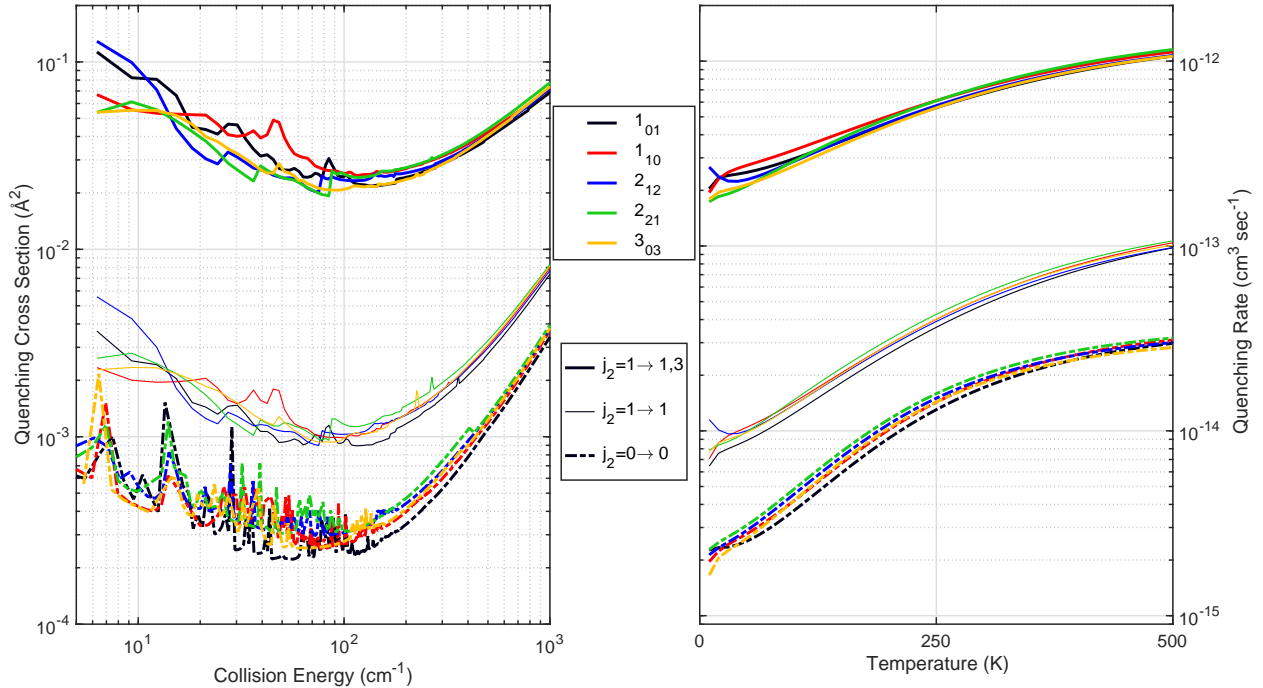


FIG. 1. **Left panel:** Quenching cross section (log scale) as a function of collision energy. Individual transitions denoted by colors and line types. **Right panel:** corresponding rates $k(T)$. Colors of the lines designate the original $v = 1$ rotational level. Line types designate the rotational basis of H_2 : Lower group: $\sigma^0(E)$; middle group, $\sigma^1(E)$, upper group $\sigma^{13}(E)$, see text.

Results are striking, as the main channel of quenching appears to go via a *simultaneous ro-vibration quenching of H₂O and a rotational excitation of H₂*, from $j_2 = 1$ upwards to $j_2 = 3$, an excitation of about 600 cm^{-1} (to be compared with a vibrational threshold at 1585 cm^{-1}), Fig. 1. Note that the $j_2 = 5$ level has an excitation threshold at 1620 cm^{-1} , above the $j_2 = 1$ levels. We made some preliminary computations of the influence of the full $j_2 = 1, 3, 5$ basis. The increase at a collisional energy of about 1500 cm^{-1} is of the order of 15%. Full investigation will be presented in future papers. The relevance of the $\Delta j_2 = +4$ is marginal at the energies considered here.

Cross sections are very significantly larger for collisions with ortho-H₂ than with para-H₂, $j_2 = 0$, an expected result, due to the non isotropy of H₂ (static quadrupole and anisotropic polarizability of H₂, allowing for anisotropic long-distance interaction). The effect is particularly large, but remains compatible with other collisions with a polar molecule^{39–41}. Here, however, vibrational quenching cross sections gain another order of magnitude *with including both $j_2 = 1$ and $j_2 = 3$ ortho rotational levels of H₂*, remaining with initial conditions at $j_2 = 1$. An earlier classical work³⁵ did not see such a strong effect at all (see their figure 4, with a monotonous decrease of rotational energy of H₂ after collision). The recent quantum paper¹⁸ did not consider these possibilities. Some hints of the importance of the rotational transitions of the projectile are seen in⁴².

Before trying to interpret the surprising results of Fig. 1, let us compare those results with previous work. We compared present rate results with earlier ones by Daniel et al.,^{43,44}, for pure rotational quenching inside the $v_b = 0$ levels, for temperatures up to 500 K, see Fig. 2. Agreement is not perfect, as expected, since Daniel et al. had a different definitions of rates and convergence (including the $j_2 > 0$ channels in their initial conditions), unrealistic for the computations here, but the important features are present, validating the code and the method.

The $j_2 = 0$ cross sections found here (lower manifold of Fig. 1) is readily found to be comparable in magnitude to those found by Stoecklin et al.,¹⁸. Secondly, in⁴⁵, a large set of transitions and temperatures was proposed, based on classical and statistical assumptions. It is difficult to compare their results with the ones presented here, as their methodology is more suited for higher T , higher initial j and makes no assumption on ortho or para state of H₂. To work qualitatively, at 300 K, we find a total rate $k(300 \text{ K}) = 3.5 \cdot 10^{-12} \text{ cm}^3 \text{ sec}$ (summed over all initial levels considered, $1 \leq j \leq 3$) and their rates amounts to $9.7 \cdot 10^{-12}$ approximately, as taken from the LAMDA database, <https://home.strw.leidenuniv.nl/moldata/> (also summed on all initial levels, $j \leq 3$). Experiment points to $1.3 \cdot 10^{-12}$, with no very clear definition of the

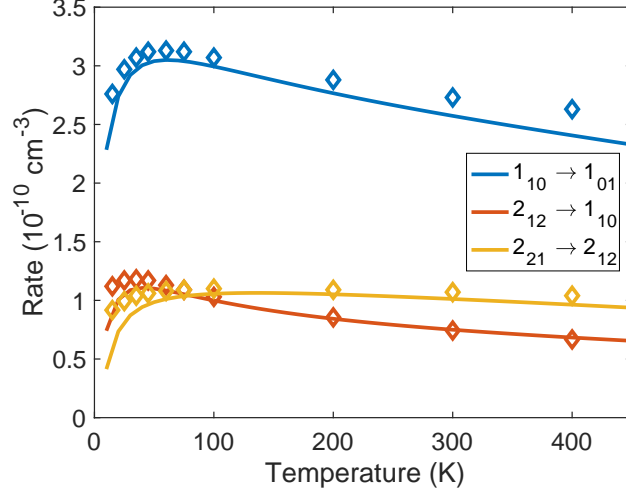


FIG. 2. Rates of de-excitation of ortho-H₂O levels in $v_b = 0$, by ortho-H₂. Diamonds, Daniel et al.⁴³; line, this work.

initial state⁴⁶. Clearly, the experiment-theory comparison must be made more precise, probably by examining pressure broadening of IR/Raman spectroscopy.

The magnitude of the rates allow us to infer the critical densities. Allowed water IR transitions are the following: $\Delta v_b = \pm 1$; $\Delta j = 0, \pm 1$, and $\Delta k_a + \Delta k_c = 0, \pm 2$. IR transitions of the low j , $v_b = 1$ occur at larger IR frequencies, hence, a relatively large *average* spontaneous emission rate $A = 24.6 \text{ sec}^{-1}$ ⁴⁷. Critical densities of H₂ are thus of the order of $n^* = 7 \cdot 10^{12} \text{ cm}^{-3}$, well within the range of atmospheric densities and outflows of aging stars. Please note that critical densities (as well as rates) are not unambiguously defined here, as many temperatures may coexist. We made use of one kinetic temperature for H₂, and summed over all quenching rates.

To disentangle various possible effects leading to the results of just outlined, we devised four different scenarios for total quenching cross sections $\sigma \equiv \sigma(v'_b = 0 \leftarrow v_b = 1)$, summed for all final rotational levels. They differ by the H₂ rotational bases and the way to treat the rotational excitation of H₂: (i) $\sigma^0(j_2 = 0)$, (ii) $\sigma^1(j_2 = 1)$, (iii) $\sigma^{13^*}(j_2 = 1, 3)$, but forbidding the $\Delta j_2 = +2$ transitions, and (iv) $\sigma^{13}(j_2 = 1, 3)$, allowing for $\Delta j_2 = +2$ transitions. They all are shown in Fig.1. We see that the σ^1 and σ^{13^*} cases are very similar, with an order of magnitude difference with σ^0 and σ^{13} . To understand the dynamics at hand, we took a twofold approach.

Firstly, we compared, for similar quenching energies, the $\Delta j_2 = 0$ (σ^{13^*}) to the $\Delta j_2 = +2$ (σ^{13}), for ro-vibrational quenching or pure rotational quenching (Fig. 3). We present results summed over all partial waves (total angular momentum), either as a function of the total collision energies

(panels (a) and (c)) or as a function of the final rotational state j of (panels(b) and (d)). Initial conditions are chosen as follows: For panels (a) and (b), initial states are $v = 1, j_1 = 1, 2, j_2 = 0$, that is initial total energy $1737.2 < E < 1861.5 \text{ cm}^{-1}$. For panels (c) and (d), we take initial levels at $v = 0$, total $1737.2 < E < 1900 \text{ cm}^{-1}$, and $9 \leq j \leq 11$. In this way, energy gap effects are kept more or less the same, whether with or without vibrational quenching.

Examining the results, for panels (a) and (b) - vibrational quenching-, we see that initial collisional energy has no peculiar feature and that final water angular momentum is weakly peaked at $j \sim 6, 7$, for both final $j_2 = 0, 2$. For panels (c) and (d) -no vibrational quenching-, initial collisional energy peaks at about 1300 cm^{-1} and diminishes strongly for smaller values. There is a propensity towards $\Delta j_2 = +2$ for small final j (large $\Delta j < 0$) and the opposite for larger final j . This goes in favour of a split of outgoing angular momentum between the two outgoing products, not seen in vibrational quenching.

The $\Delta j_2 = +2$ channel dominates the picture for vibrational quenching by at least one order of magnitude when the channels are opened (right of blue threshold line, panels (a), (c), $j \leq 10$, panels (b),(d)). It is not the case for pure rotational quenching. It is all the more remarkable that for the $v = 0 \rightarrow 0$ quenchings, the loss of angular momentum is much higher, with $j_{\text{ini}} \geq 9$. H_2 carrying away angular momentum is not the main effect here. Also, energy loss is similar, hence energy gap effects are ruled out in the comparison. Inside the $v_b = 0$ vibrational level, we find a weak dominance of the $\Delta j_2 = 0$ transitions, similar to what Daniel et al. found (Figure 1 of reference Daniel *et al.*⁴⁰)

Secondly, we compute and draw the ro-vibrational channels that are used for the dynamical propagation, as a function of R . We consider the diagonal part of the $W(R)$ matrix (equation 1) as a diabatic image and its eigenvalues, $\text{eig}[W(R)]$ as an adiabatic image, Fig. 4. Plots are for total $J = 2, j \leq 3$, a good compromise between generality (the $J = 6$ or 12 are very similar in appearance; adding j channels do not change the picture) and as small a number of channels as possible, for sake of readability. We see straightforwardly that in the case of $j_2 = 0$, crossings between incoming black $v_b = 1, j_2 = 0$ channels and outgoing red $v_b = 0, j_b = 0$ channels are limited to the repulsive wall, at very high collision energies. Cross sections are exceedingly small, but increase rapidly once the crossings are open, energy-wise. Exchanges between the various $v_b = 0$ channels is possible, seemingly at all energies and distances. The $j_2 = 1$ case does not fundamentally change the picture. There are crossings (diabatic picture) or avoided crossings for energies lower than threshold, at $R \sim 8$ Bohr, sufficiently effective to insure some transfer

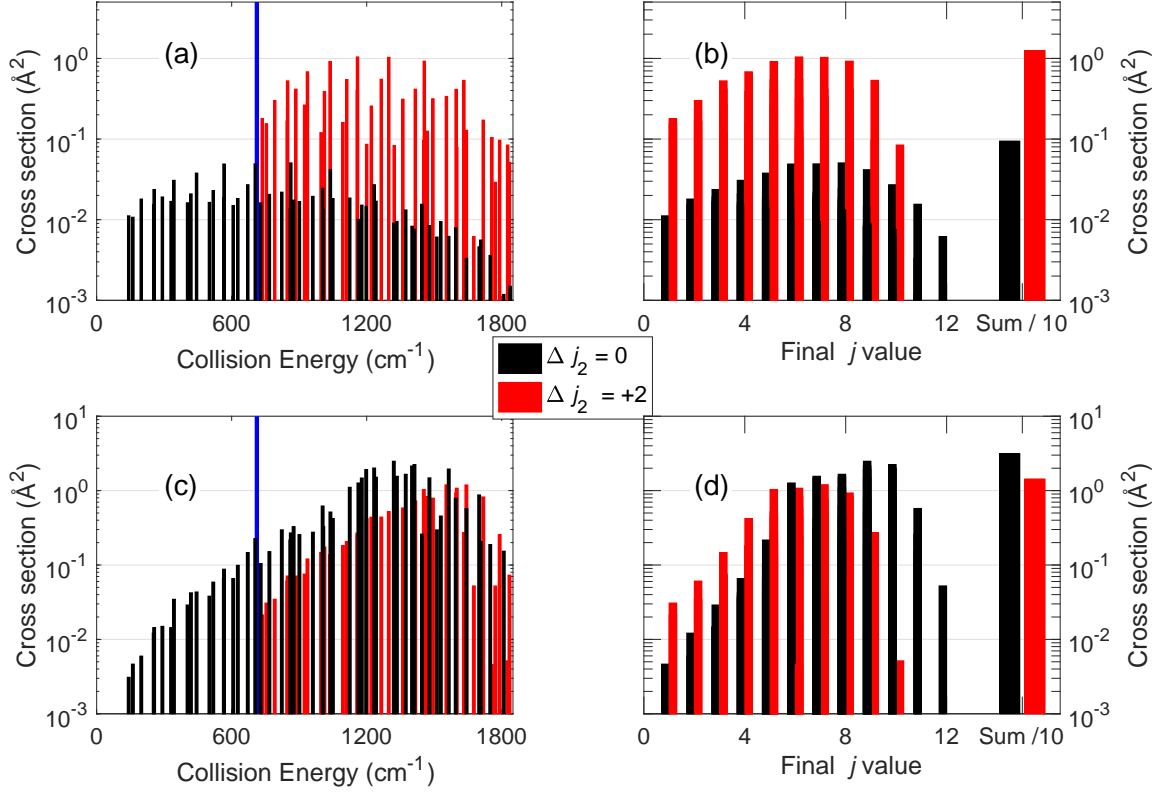


FIG. 3. Comparison between rotational quenching, for transition without excitation of H_2 ($\Delta j_2 = 0$, black bars), and with excitation of H_2 ($\Delta j_2 = +2$, red bars). Total angular momentum summed, $0 \leq J \leq 32$. Panels (a), (c), cross sections as a function of collision energy. Blue vertical line indicate the $\Delta j_2 = +2$ threshold. Panels (b), (d), cross sections as a function of final H_2O principal rotation quantum number j . $j = 11, 12$ are above threshold for $\Delta j_2 = +2$ excitation. Panels (a), (b), rovibrational quenching (summed for all initial $\nu_b = 1$, $j \leq 2$ and all final $\nu_b = 0$, $E_i > E_f$). Panels (c), (d), pure rotational quenching (summed for all initial $\nu_b = 0$, $E \geq 1585 \text{ cm}^{-1}$ and all final $\nu_b = 0$, $E_i > E_f$). Last bars in panels (b), (d) sum all contributions.

of probability amplitude. Note that the higher energy, $R \sim 10$ avoided crossings should be less efficient, in a Landau-Zener picture, because of the large slope difference between the adiabats.

Picture changes dramatically for the third case, $j = 1, 3$, $\Delta j_2 = 0, +2$, two lower panels. If we detail the diabatic picture (lower left panel), we see (i) that the $\nu_b = 1$, $j_2 = 1$ channels (black) are allowed to cross the $\nu_b = 1$, $j_2 = 3$ channels (green) in the $R \sim 10$ region, allowed energy-wise. Then, (ii), the probability amplitude, divided into many channels, crosses a large manifold of

$\nu_b = 0, j_2 = 3$ (magenta) or $\nu_b = 0, j_2 = 1$ (red) channels, at $R \sim 7 - 10$, in the diabatic picture, allowing for probability amplitude to flow out on the whole manifold. This picture accounts for the increase of inelastic cross sections and rates, but without any propensity rule apparent. If we turn to the adiabatic picture (lower right panel), we see that the magenta levels have a series of avoided crossings with the incoming channels at all distances. The larger number of magenta adiabats, their avoided crossings at all distances, including the larger R distances just below threshold may be enough to point to the propensity rules observed in the quantum dynamics.

To conclude the discussion, we found it worthwhile to have a first glimpse of what the situation might be, for a heavy-heavy collision of utmost atmospheric importance, $\text{H}_2\text{O} \cdots \text{N}_2$. Even if a very recent rigid bender PES exists,⁴⁸ fits are not in line of what is needed here, and we look only for some very qualitative results. We used the same PES as before (same symmetry of the system); it is all the more justified that V_{\min} remains similar (about 250-300 cm^{-1}). This tN2 (toy- N_2) computation of diabats and adiabats is performed exactly similarly, with the two following changes: $B_{\text{N}_2} = 2.01 \text{ cm}^{-1}$ and reduced mass $\mu = 10.9565$. While ortho and para $^{14}\text{N}_2$ have the opposite meaning from $^1\text{H}_2$ (because of the bosonic character of ^{14}N , of nuclear spin $I = 1$), we did not change the j_2 values.

Fig. 5 show the results, with the same conventions as in Fig. 4. Without any supposition for the dynamics, we see that the same effects persist, namely, a large increase of avoided crossings, from $j_2 = 1$ to $j_2 = 1, 3$. In this tN2 case we have a large decrease (factor of 25) of the projectile rotational constant (here below the target rotational constants), but the vibrational gap remains. The large fans of adiabats should allow for higher cross sections, because of the various energy scales involved.

One should not take those tN2 computations for more than indications. In particular, they do not claim for any convergence. However, they should be a warning before deciding whether a cold molecule collision vibrational quenching proceeds classically for all the energy sectors considered. In low T physics, it could be fine structure, vibration, rotation, and each could operate in a very different way.

Foseca dos Santos et al.⁴⁹ studied some time ago the $\text{H}_2 \cdots \text{H}_2$ system, considering ro-vibrational de-excitation cross sections, for both ortho-para and ortho-ortho collisions, at mostly low collisions energy (up to 100 K). Since in the present work, molecules are distinguishable, the comparison is more relevant in the ortho- $\text{H}_2 \cdots$ para- H_2 case, as the ortho-ortho case presents resonances and symmetry effects absent here. We found here that the dominant channel for vibrational quenching

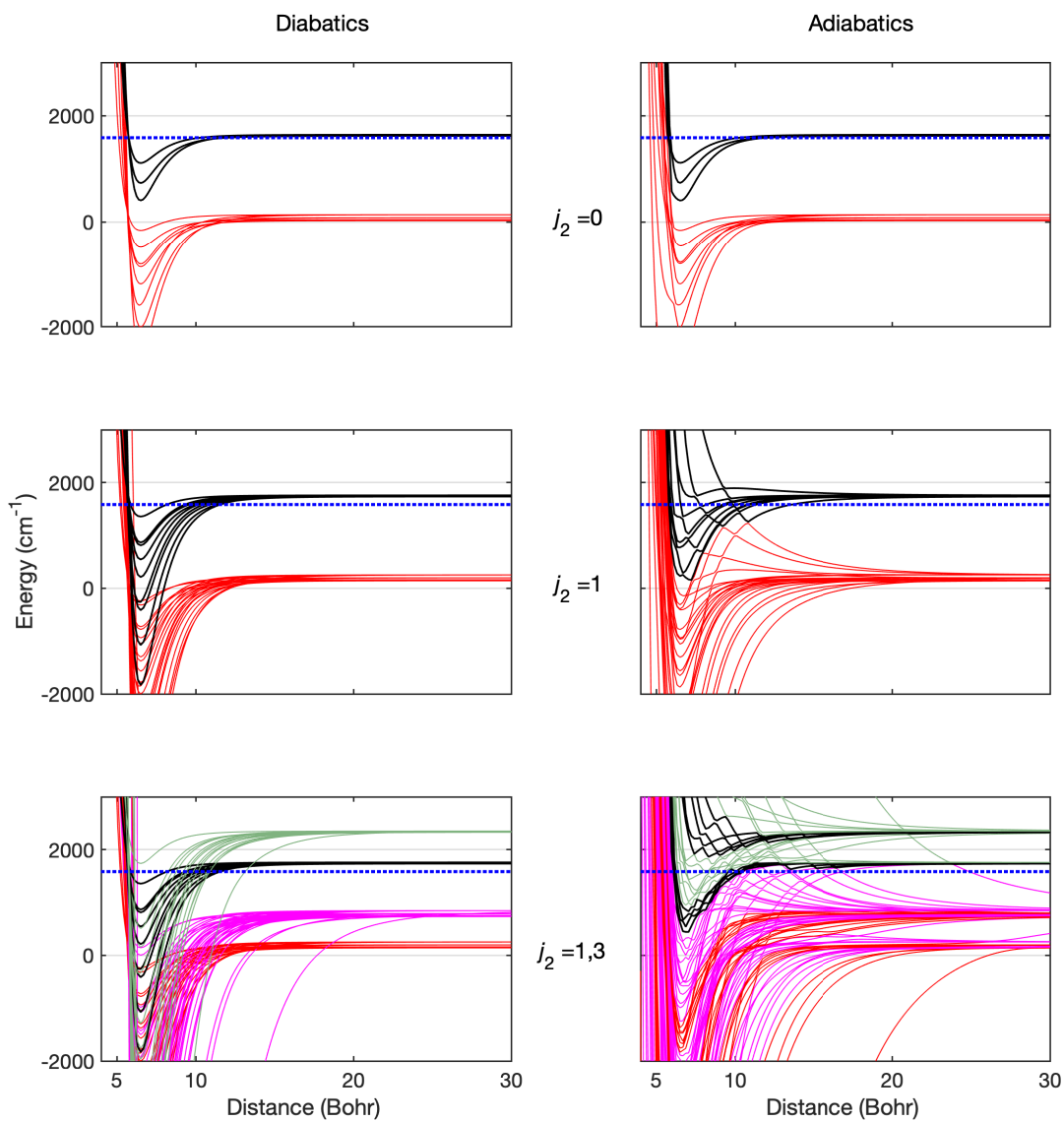


FIG. 4. Diabats and adiabats for the $\text{H}_2\text{O}\cdots\text{H}_2$ collision. Left panels, diabats (diagonal part of the W matrix, Eq.(1)), as a function of intermolecular distance. Right panels, adiabats (eigenvalues of the W matrix, Eq.(1)) as a function of intermolecular distance. Asymptotic quantum numbers : black lines: $\nu_b = 1$, $j_2 = 0$ or $j_2 = 1$; red lines $\nu_b = 0$, $j_2 = 0$ or $j_2 = 1$; light green $\nu_b = 1$, $j_2 = 3$; magenta $\nu_b = 1$, $j_2 = 1$. Blue dashed line: $\nu_b = 1$, ortho H_2O threshold. See discussion in the text.

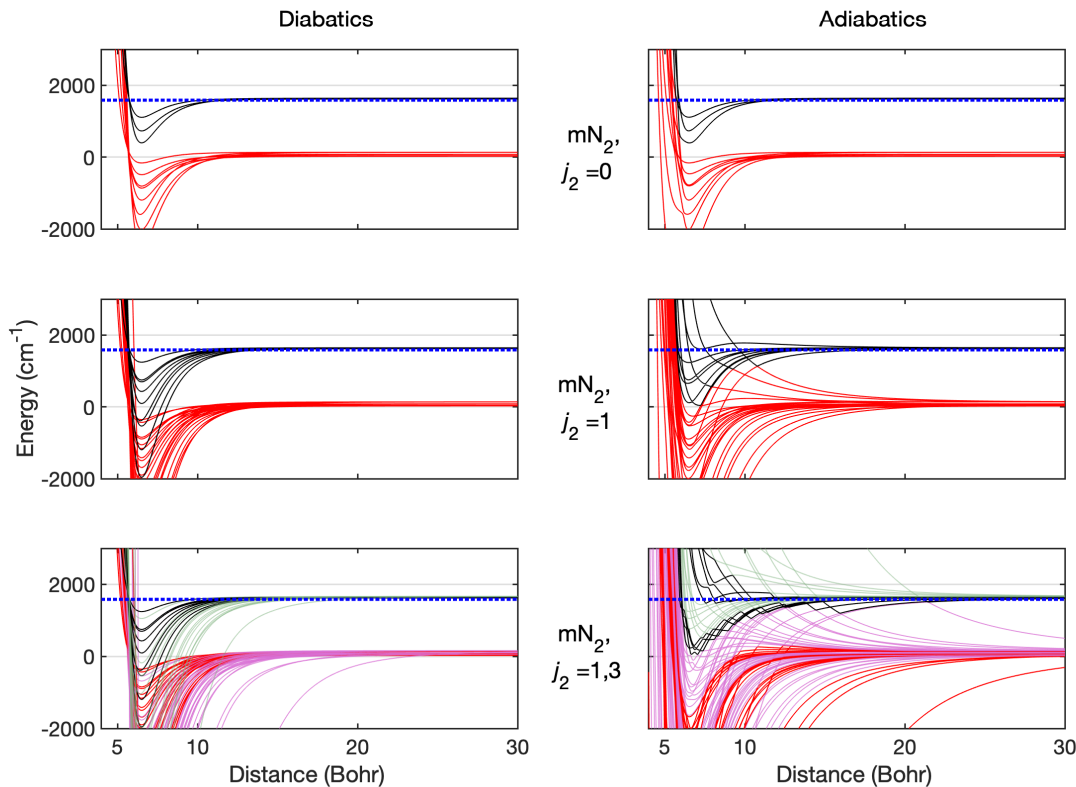


FIG. 5. Diabats and adiabats for the $\text{H}_2\text{O} \cdots t\text{N}_2$ collision. Left panels, diabats (diagonal part of the W matrix, Eq.(1)), as a function of intermolecular distance. Right panels, adiabats (eigenvalues of the W matrix, Eq.(1)) as a function of intermolecular distance. Asymptotic quantum numbers : black lines: $\nu_b = 1$, $j_2 = 0$ or $j_2 = 1$; red lines $\nu_b = 0$, $j_2 = 0$ or $j_2 = 1$; light green $\nu_b = 1$, $j_2 = 3$; magenta $\nu_b = 1$, $j_2 = 1$. Blue dashed line: $\nu_b = 1$, ortho H_2O threshold. See discussion in the text.

is $j_2 = 1 \rightarrow 3$, irrespective of the collision energy (Fig. 1), thereby reducing the amount of energy to be transferred, independently of angular momentum transfer. The situation is somewhat different for $\text{H}_2 \cdots \text{H}_2$: for the 1001 collision, (notation: $\nu_1 j_1 \nu_2 j_2$; 1,2 the two H_2 molecules), the dominant channel by far is $1001 \rightarrow 0011$, conserving the rotational angular momentum. The analogous $1001 \rightarrow 0201$ is about a factor 5 smaller. An adiabatic analysis similar would sort out the differences, that may be due to the paucity of adiabatic levels (two rods, $B = 60 \text{ cm}^{-1}$, far fewer channels). The ortho-ortho case is quite different from the case analyzed here, as resonances and symmetry effects may be dominant effects.

We have shown that the vibrational quenching behaves in a very different way than the rotational quenching, because of the organization of the ro-vibrational quantum levels. Approximations not allowing rotational (and possibly vibrational) excitation of the projectile may be underestimating the actual rates by a large amount, here by a factor of 10 at least. Ignoring the nuclear symmetry of the projectile would also lead to large over-estimation of rates. The results presented here suggest that ro-vibrational quenching by light atoms or by molecules at their zero angular momentum level is fundamentally different from non-zero angular momentum, because *both* long distance and short distance behaviours of the diabatic or adiabatic channels.

The atmospheric vibrational quenching, driving the IR radiation redistribution towards kinetic energy should thus be carefully conducted in a manner allowing for all the essential angular momenta to be properly taken into account. Probing line shapes via IR/Raman spectroscopy is all the more relevant and will be the object of further theoretical investigations. The critical density found for ro-vibrational quenching points to high atmospheres of stars or planets, to dense parts of late stage stars, confirming that the 658 GHz maser line finds its origin in the unbalance of collisions and optical rates for the low j , $v_b = 1$ levels.

As the similarity of rates for the various initial states in our limited range of initial water angular momentum suggests, it is worthwhile to develop specific ways of treating theoretically ro-vibrational quenching, as was done long ago for rotational quenching, to ease the burden of computation time. In this way, the all-important collision systems for our atmosphere ($\text{H}_2\text{O}/\text{CO}_2/\text{CH}_4 \cdots \text{N}_2/\text{O}_2$) will become doable by relevant quantum methods.

ACKNOWLEDGMENTS

The author thanks J. Hutson and M. Gonzalez-Martinez (Durham U.) for setting up the relevant basis sets for vibrational quenching with Molscat conventions, and A. Faure (Grenoble U.) for providing details of the potential surface. Enlightening discussion and support from O. Dulieu and N. Bouloufa are gratefully acknowledged. Computations presented in this paper were performed with grants A0060810769/A0080810769 on the ADA and JEAN-ZAY CNRS super-computers, hosted at IDRIS.

DATA AVAILABILITY

The potential energy surface has been published earlier³⁴. The Fortran subroutines for computing the full surface are available from the author upon reasonable request. The quenching data presented here are computed from a large body of raw data, which were generated at the CNRS-IDRIS large facility. Derived data supporting the findings of this study are available from the author upon reasonable request.

REFERENCES

- ¹J. Hartmann, C. Boulet, and D. Robert, *Collisional Effects on Molecular Spectra* (Elsevier, 2008).
- ²R. Hellmann, *Journal of Chemical & Engineering Data* **65**, 4712 (2020), <https://doi.org/10.1021/acs.jced.0c00605>.
- ³N. J. Brown, L. A. Bastien, and P. N. Price, *Progress in Energy and Combustion Science* **37**, 565 (2011).
- ⁴P. J. Dagdigian and M. H. Alexander, *The Journal of Chemical Physics* **139**, 194309 (2013), <https://doi.org/10.1063/1.4829681>.
- ⁵L. D. Carr, D. DeMille, R. V. Krems, and J. Ye, *NEW JOURNAL OF PHYSICS* **11** (2009), 10.1088/1367-2630/11/5/055049.
- ⁶M.-G. Hu, Y. Liu, M. A. Nichols, L. Zhu, G. Quéméner, O. Dulieu, and K.-K. Ni, *Nature Chemistry* **13**, 435 (2021).
- ⁷E. Roueff and F. Lique, *Chemical Reviews* **113**, 8906 (2013), [arXiv:1310.8259](https://arxiv.org/abs/1310.8259) [physics.chem-ph].
- ⁸T. Karman, M. A. J. Koenis, A. Banerjee, D. H. Parker, I. E. Gordon, A. van der Avoird, W. J. van der Zande, and G. C. Groenenboom, *Nature Chemistry* **10**, 549 (2018).
- ⁹F. F. S. van der Tak, F. Lique, A. Faure, J. H. Black, and E. F. van Dishoeck, *Atoms* **8**, 15 (2020), [arXiv:2004.11230](https://arxiv.org/abs/2004.11230) [astro-ph.GA].
- ¹⁰J. Cernicharo, J. D. Gallego, J. A. López-Pérez, F. Tercero, I. Tanarro, F. Beltrán, P. de Vicente, K. Lauwaet, B. Alemán, E. Moreno, V. J. Herrero, J. L. Doménech, S. I. Ramírez, C. Bermúdez, R. J. Peláez, M. Patino-Esteban, I. López-Fernández, S. García-Álvaro, P. García-Carreño, C. Cabezas, I. Malo, R. Amils, J. Sobrado, C. Diez-González, J. M. Hernández, B. Tercero,

- G. Santoro, L. Martínez, M. Castellanos, B. Vaquero Jiménez, J. R. Pardo, L. Barbas, J. A. López-Fernández, B. Aja, A. Leuther, and J. A. Martín-Gago, *Astron. Astroph.* **626**, A34 (2019).
- ¹¹S. Manigand, J. K. Jørgensen, H. Calcutt, H. S. P. Müller, N. F. W. Ligterink, A. Coutens, M. N. Drozdovskaya, E. F. van Dishoeck, and S. F. Wampfler, *Astron. Astroph.* **635**, A48 (2020), arXiv:2001.06400 [astro-ph.SR].
- ¹²Greenwood, A. J., Kamp, I., Waters, L. B. F. M., Woitke, P., and Thi, W.-F., *A&A* **631**, A81 (2019).
- ¹³E. F. van Dishoeck, L. E. Kristensen, J. C. Mottram, A. O. Benz, E. A. Bergin, P. Caselli, F. Herpin, M. R. Hogerheijde, D. Johnstone, R. Liseau, B. Nisini, M. Tafalla, F. F. S. van der Tak, F. Wyrowski, A. Baudry, M. Benedettini, P. Bjerkerli, G. A. Blake, J. Braine, S. Bruderer, S. Cabrit, J. Cernicharo, Y. Choi, A. Coutens, T. de Graauw, C. Dominik, D. Fedele, M. Fich, A. Fuente, K. Furuya, J. R. Goicoechea, D. Harsono, F. P. Helmich, G. J. Herczeg, T. Jacq, A. Karska, M. Kaufman, E. Keto, T. Lamberts, B. Larsson, S. Leurini, D. C. Lis, G. Melnick, D. Neufeld, L. Pagani, M. Persson, R. Shipman, V. Taquet, T. A. van Kempen, C. Walsh, S. F. Wampfler, U. Yıldız, and WISH Team, *Astron. Astroph.* **648**, A24 (2021), arXiv:2102.02225 [astro-ph.GA].
- ¹⁴K. M. Menten and K. Young, *Astrophys. J. Lett.* **450**, L67 (1995).
- ¹⁵A. V. Nesterenok, *Monthly Not. Royal Astron. Soc.* **449**, 2875 (2015), arXiv:1503.07041 [astro-ph.SR].
- ¹⁶A. Baudry, E. M. L. Humphreys, F. Herpin, K. Torstensson, W. H. T. Vlemmings, A. M. S. Richards, M. D. Gray, C. De Breuck, and M. Olberg, *Astron. Astroph.* **609**, A25 (2018), arXiv:1711.02350 [astro-ph.SR].
- ¹⁷A. Faure, N. Crimier, C. Ceccarelli, P. Valiron, L. Wiesenfeld, and M. L. Dubernet, *Astron. Astroph.* **472**, 1029 (2007), arXiv:0708.0345.
- ¹⁸T. Stoecklin, O. Denis-Alpizar, A. Clergerie, P. Halvick, A. Faure, and Y. Scribano, *Journal of Physical Chemistry A* **123**, 5704 (2019).
- ¹⁹T. Stoecklin, L. D. Cabrera-González, O. Denis-Alpizar, and D. Páez-Hernández, *The Journal of Chemical Physics* **154**, 144307 (2021), <https://doi.org/10.1063/5.0047718>.
- ²⁰B. Drouin and L. Wiesenfeld, *Phys. Rev. A* **86**, 022705 (2012).
- ²¹A. Faure, L. Wiesenfeld, B. J. Drouin, and J. Tennyson, *J. Quant. Spec. Rad. Trans.* **116**, 79 (2013).

- ²²A. Bergeat, S. Morales, C. Naulin, L. Wiesenfeld, and A. Faure, *Physical Review Letters* **125**, 143402 (2020).
- ²³J. Loreau, F. Lique, and A. Faure, *Astrophys. J. Lett.* **853**, L5 (2018), arXiv:1801.02514 [astro-ph.IM].
- ²⁴A. Faure and L. Wiesenfeld, *J. Chem. Phys.* **121**, 6771 (2004).
- ²⁵A. M. Arthurs and A. Dalgarno, *Proceedings of the Royal Society of London Series A* **256**, 540 (1960).
- ²⁶S. Green and P. Thaddeus, *Astrophys. J.* **191**, 653 (1974).
- ²⁷S. Green, *Chemical Physics Letters* **47**, 119 (1977).
- ²⁸T. R. Phillips, S. Maluendes, and S. Green, *J. Chem. Phys.* **102**, 6024 (1995).
- ²⁹D. R. Flower, G. Bourhis, and J. Launay, *Computer Physics Communications* **131**, 187 (2000).
- ³⁰M.-L. Dubernet, M. H. Alexander, Y. A. Ba, N. Balakrishnan, C. Balança, C. Ceccarelli, J. Cernicharo, F. Daniel, F. Dayou, M. Doronin, F. Dumouchel, A. Faure, N. Feautrier, D. R. Flower, A. Grosjean, P. Halvick, J. Kłos, F. Lique, G. C. McBane, S. Marinakis, N. Moreau, R. Moszynski, D. A. Neufeld, E. Roueff, P. Schilke, A. Spielfiedel, P. C. Stancil, T. Stoecklin, J. Tennyson, B. Yang, A.-M. Vasserot, and L. Wiesenfeld, *Astron. Astroph.* **553**, A50 (2013).
- ³¹J. M. Hutson and S. Green, “MOLSCAT computer code, version 14 (1994), distributed by collaborative computational project no. 6 of the engineering and physical sciences research council (uk),” (1994).
- ³²M. H. Alexander and D. E. Manolopoulos and H.-J. Werner and B. Follmeg and P. J. Dagdigian, “Hibridon package.”
- ³³M. P. Ziemkiewicz, C. Pluetzer, D. J. Nesbitt, Y. Scribano, A. Faure, and A. van der Avoird, *JOURNAL OF CHEMICAL PHYSICS* **137** (2012), 10.1063/1.4732581.
- ³⁴P. Valiron, M. Wernli, A. Faure, L. Wiesenfeld, C. Rist, S. Kedžuch, and J. Noga, *J. Chem. Phys.* **129**, 134306 (2008).
- ³⁵A. Faure, L. Wiesenfeld, M. Wernli, and P. Valiron, *J. Chem. Phys.* **123**, 104309 (2005).
- ³⁶E. Kyrö, *Journal of Molecular Spectroscopy* **88**, 167 (1981).
- ³⁷D. E. Manolopoulos, *J. Chem. Phys.* **85**, 6425 (1986).
- ³⁸A. Baudry, E. M. L. Humphreys, F. Herpin, K. Torstensson, W. H. T. Vlemmings, A. M. S. Richards, M. D. Gray, C. De Breuck, and M. Olberg, *Astron. Astroph.* **609**, A25 (2018), arXiv:1711.02350 [astro-ph.SR].
- ³⁹B. Yang, H. Perera, N. Balakrishnan, R. C. Forrey, and P. C. Stancil, *Journal of Physics B: Atomic, Molecular and Optical Physics* **39**, S1229 (2006).

- ⁴⁰F. Daniel, M. L. Dubernet, F. Pacaud, and A. Grosjean, *Astron. Astroph.* **517**, A13 (2010).
- ⁴¹N. Bouhafs, C. Rist, F. Daniel, F. Dumouchel, F. Lique, L. Wiesenfeld, and A. Faure, *Monthly Not. Royal Astron. Soc.* **483**, 4639 (2019).
- ⁴²B. Yang, P. Zhang, C. Qu, P. Stancil, J. Bowman, N. Balakrishnan, and R. Forrey, *Chemical Physics* **532**, 110695 (2020).
- ⁴³F. Daniel, M. L. Dubernet, and A. Grosjean, *Astron. Astroph.* **536**, A76 (2011).
- ⁴⁴F. Daniel, M. L. Dubernet, M. Doronin, L. Nenadovic, and J. Bureau, in *The Molecular Universe*, Vol. 280, edited by J. Cernicharo and R. Bachiller (2011) p. 395.
- ⁴⁵A. Faure and E. Josselin, *Astron. Astroph.* **492**, 257 (2008).
- ⁴⁶P. F. Zittel and D. E. Masturzo, *J. Chem. Phys.* **95**, 8005 (1991).
- ⁴⁷R. J. Barber, J. Tennyson, G. J. Harris, and R. N. Tolchenov, *Monthly Not. Royal Astron. Soc.* **368**, 1087 (2006), arXiv:astro-ph/0601236 [astro-ph].
- ⁴⁸L. Wang, X.-L. Zhang, Y. Zhai, M. Nooijen, and H. Li, *The Journal of Chemical Physics* **153**, 054303 (2020), <https://doi.org/10.1063/5.0009098>.
- ⁴⁹S. F. d. Santos, N. Balakrishnan, S. Lepp, G. Quéméner, R. C. Forrey, R. J. Hinde, and P. C. Stancil, *The Journal of Chemical Physics* **134**, 214303 (2011), <https://doi.org/10.1063/1.3595134>.